1988-05-01

Many-body embedded-atom potential for describing the energy and angular distributions if Rh atoms desorbed from ion-bombarded Rh(111)

Garrison, B. J.

American Physical Society

Many-body embedded-atom potential for describing the energy and angular distributions of Rh atoms desorbed from ion-bombarded Rh{111}

B. J. Garrison, N. Winograd, D. M. Deaven, and C. T. Reimann
Department of Chemistry, Pennsylvania State University, University Park, Pennsylvania 16802

D. Y. Lo and T. A. Tombrello
Division of Physics, Mathematics and Astronomy, California Institute of Technology, Pasadena, California 91125

D. E. Harrison, Jr.
Department of Physics and Chemistry, Naval Postgraduate School, Monterey, California 93943

M. H. Shapiro
Division of Physics, Mathematics and Astronomy, California Institute of Technology, Pasadena, California 91125 and Department of Physics, California State University, Fullerton, California 92634
(Received 8 September 1987; revised manuscript received 21 December 1987)

In this paper, we show that many-body interactions are important for describing the energy- and angle-resolved distributions of neutral Rh atoms ejected from keV-ion-bombarded Rh{111}. We compare separate classical-dynamics simulations of the sputtering process assuming either a many-body potential or a pairwise additive potential. The many-body potential is constructed using the embedded-atom method to describe equilibrium properties of the crystal, parameters from the Molière potential to describe close encounters between energized atoms, and parameters from a Rh_2 potential to aid the description of the desorption event. The most dramatic difference between the many-body potential and the pair potential is in the predicted kinetic energy distributions. The pair-potential kinetic energy distribution peaks at ~ 2 eV, whereas the many-body potential predicts a broader peak at ~ 4 eV, giving much better agreement with experiment. This difference between the model potentials is due to the predicted nature of the attractive interaction in the surface region through which all ejecting particles pass. Variations of the many-body-potential parameters are examined in order to ascertain their effect on the predicted energy and angular distributions. A specific set of parameters has been found which leads to excellent agreement with recent experimental trajectory measurements of desorbed Rh atoms.

I. INTRODUCTION

The development of many-body interaction potentials to describe the forces among large ensembles of atoms (e.g., solids or liquids) is presently in its infancy. Over the years investigators have sought to find systems and scattering regimes where these types of potential functions may be expressed in a mathematically tractable form. One such process is the ejection of atoms due to 500–5000 eV particle bombardment of solids (i.e., sputtering). In this case atoms are ejected from the solid with a kinetic energy $E_{\rm kin}$ distribution which maximizes at 2–10 eV and which decreases as $E_{\rm kin}^{-2}$ up to energies which are a significant fraction of the energy of the incident particle. The complex atomic motion subsequent to the ion-bombardment event is clearly initiated by close encounters between colliding atoms in the solid. These types of interactions may provide an excellent model system for developing an accurate many-body interaction potential.

Since 1960 particle bombardment events have been simulated by computer models which assume pairwise additive potential functions.[1] The simplest approach is to assume that the interactions are purely repulsive and that the collision dynamics can be described by the binary collision approximation where each particle is allowed to interact with only the nearest atom at a given time.[2] On the other hand, we believe that at the energies at which most particles eject, 2–10 eV, simultaneous interactions are not negligible and in fact play a dominant part in controlling the collision dynamics.[3–7] Due to computational restrictions, our full lattice descriptions have thus far been limited to pairwise additive potentials, although attractive interactions have been included.

These potentials have been quite successful at elucidating mechanisms of particle ejection, and at allowing calculation of semiquantitative aspects of the sputtering process.[4] However, a quantitative comparison between theory and experiment has been hindered by a scarcity of detailed experimental data. The computer simulations using single crystal targets yield direct information concerning the trajectories of ejecting neutral atoms. Early experiments were capable only of examining energy-integrated or angle-integrated neutral distributions from damaged targets or of examining trajectories of secondary ions. The motion of the ions could be detected with

high sensitivity but the distributions had to be corrected for the image forces created by the charge.[8] A new method based on the multiphoton resonance of neutral atoms after they have desorbed from the target surface has recently been developed. The technique is capable of measuring the energy- and angle-resolved neutral (EARN) distributions of sputtered atoms[9–11] with sensitivity sufficient to avoid surface damage. These experiments provide the best trajectory data yet available and force a critical test of assumed interaction potentials and scattering dynamics.

In a previous study we described the EARN distribution of Rh atoms ejected from Rh{111} with a computer simulation using pairwise additive interaction potentials.[7] Although the overall trends of azimuthal anisotropies and relative intensities of angular peaks were well described, the position of the peaks and the peak widths in both the polar angle and energy distributions differed between the experimental and calculated results. Variation of the parameters in the potential within physically reasonable bounds did not significantly improve agreement.

In this paper we present the first use of many-body potentials to describe the ejection of atoms from solid surfaces due to keV ion bombardment. The potential is derived from the embedded-atom method (EAM) of Daw and Baskes.[12,13] This many-body potential significantly improves the agreement between the measured and calculated peak positions and widths in the energy and angular distributions of Rh atoms ejected from Rh{111}. Several variations of the potential are examined to determine the influence of selected parameters on the calculated distributions. The results show that the EAM approach yields excellent agreement with the expected kinetic energy distributions for all potentials tested. However, the angular distributions are influenced by a number of parameters. We especially examine the difference between calculated trajectories in the surface region when using an EAM potential as compared to earlier pair-potential calculations.

II. DESCRIPTION OF THE CALCULATION

Our prescription for modeling the ion-bombardment process has been described in detail elsewhere for the Ar^+ ion bombardment of Rh{111}.[7] The critical difference in the present study is that a many-body EAM potential has been used to describe the Rh metal interaction. The EAM utilizes an ion-core representation of the metal atom embedded into the surrounding electron sea.[12–14] The energy for the ith atom is given by

$$E_i = F\left[\rho_i = \sum_j \rho_{\text{atomic}}(r_{ij})\right] + \tfrac{1}{2}\sum_j \phi(r_{ij}) , \qquad (1)$$

where r_{ij} is the distance between the ith atom and the jth atom. The first term is the embedding function, which is the energy of the interaction of the ion core with the electron sea of density ρ_i. The embedding function is characteristic of a particular atom type and is assumed not to depend on the source of the electron density. Thus the embedding function for Rh is transferrable from one environment to another if the electron density is known. For convenience, this density is assumed to be the instantaneous sum of the atomic electron densities of the other atoms at the position of the atom of interest. Since these densities depend only on the distance between the atoms forces are easily extracted for dynamics simulations. The second term is short ranged and is the ion-core repulsion at a distance of separation, r_{ij}, of the two cores. It is of interest that the EAM has been successfully applied to describing bulk properties at thermal energies and even to predicting surface reconstructions.[12,16] However, to our knowledge it has not been applied to systems where parts of the solid actually dissociate as is the case with evaporation and ion-induced desorption.

The embedding functions are empirically derived, and as a consequence the $F(\rho)$ and the $\phi(r)$ terms must be systematically evaluated. Foiles, Baskes, and Daw have developed a prescription for fitting these functions to equilibrium properties of the metal of interest.[14] To describe the ion-bombardment process, it is necessary to consider that atomic positions may be displaced far from their equilibrium values. The energetics of an atom as it ejects from the surface, and the details of close encounters with other atoms are also important, indicating that a slightly different fitting procedure is necessary. Our approach, as described in the Appendix, is basically the same as that of Foiles, *et al.* except that the potential form also incorporates parameters appropriate for Rh_2 (i.e., in the low-density regime) and for the repulsive wall which is important during close encounters (i.e., in the very-high-density regime).

A number of embedding functions for Rh with different repulsive walls and attractive regions were used for simulations of the EARN distributions. We found that, to reproduce the experimental energy distributions, the value of the surface binding energy for the EAM potential must be ≥ 5 eV. Here we have chosen to use Eq. (1) to define the energy of an atom in the surface region. This definition results in a value of the surface binding energy which is less than the true energy cost to remove an atom from the substrate.[17–19] Since the density regimes appropriate for the surface region and for Rh_2 overlap, we are not able at this stage to utilize the spectroscopic constants for the dimer and also obtain a surface binding energy of > 5 eV. By adjusting these values, however, as described in the Appendix, potential forms were found that fit the experimental angular distributions in the 20–50 eV range (EAM-C), and in the 10–20 eV range (EAM-D). Two other potentials, (EAM-A and EAM-B), that are approximately linear combinations of EAM-C and EAM-D, are also tested in this work. The details of the determination of EAM-A are given in the Appendix. In summary, our present strategy for finding a representative many-body potential consists of utilizing the previously developed formalism to calculate forces of atoms near equilibrium positions, and then semiempirically adjusting the potential shapes appropriate for close encounters and for dissociations until the function provides a physically accurate representation of the experimental results.

The EAM form of the total potential energy expression can be obtained in a purely empirical way,[20] but its valid-

ity can be more rigorously justified by deriving it as an approximation method in formal effective-medium theory.[21] The derivation is based on the replacement of the effective-medium expression for the energy of an atom embedded in an arbitrary host with the energy of the atom in a homogeneous electron gas. In the effective-medium prescription, the density is determined self-consistently. In the EAM the density of the homogeneous electron gas is used to approximate the true density. The EAM replaces a functional of the host electron density with a function of the electron density at a point. In this context the EAM "embedding function" is interpreted as the cohesive energy of the atom in jellium. The pairwise additive term can be obtained with first-order perturbation theory on the jellium system with an external potential representing the host.[21] For proper physical interpretation, the EAM "embedding function" must have a low-density limit of zero, unlike the hypothetical jellium limit which reflects the formation of a negative ion for chemically active elements in the limit of extremely low jellium density. We note that Norskov[22,23] has shown that a second correction term reflects the difference between the one-electron spectrum of an atom embedded in jellium and the same atom embedded in a solid host. This correction accounts for the hybridization or band energy resulting from the formation of relatively delocalized states in the solid. The keV ion-bombardment process studied in this work causes severe local disruptions of the equilibrium lattice and leads to atomic desorption. Since the hybridization energy during this process is likely to differ significantly from that of a uniform lattice, the knowledge of the uniform lattice one-electron spectrum is insufficient to correct for hybridization effects during the desorption event. In principle, this correction could be made by calculating the instantaneous band structure at each simulation timestep,[24] but this completely circumvents any computational advantages of the semiempirical form. Therefore, we employ the EAM form [Eq. (1)] in its original form as a parametrized mathematical representation of the potential energy hypersurface which includes many-body terms in a convenient but theoretically justified manner.

III. RESULTS AND DISCUSSION

Highly reliable trajectory information is now available over all angle and kinetic energy domains for Rh atoms desorbed from ion-bombarded Rh{111}. To act as a standard subset of reference data for our computer simulations, we have chosen to select angle-integrated kinetic energy distributions of the ejected Rh atoms and polar angle distributions along three azimuthal directions of the {111} crystal face (Fig. 1) for three secondary particle energy ranges. These data, as well as computer simulations of these trajectories using pair potentials, have been reported previously.[7]

The most dramatic difference observed between the pair potential and the EAM potential is in the predicted distributions arising in the angle-integrated energy distributions. As shown in Fig. 2, the distributions from experiment and calculations using the EAM-A interaction

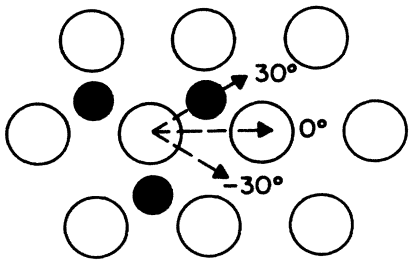

FIG. 1. Rh{111} crystal face. The open circles are first-layer atoms and the solid circles represent second-layer atoms. The azimuthal directions of $\phi = -30°$, 0°, and 30° are shown.

are in excellent agreement while the calculated distribution using pair potentials is significantly different. The peaks in the polar angle distributions as calculated from the EAM-A potential (Fig. 3) are also found to increase by about 10° from those predicted by the pair potentials. The improved agreement in the energy distributions is fairly consistent among all the EAM potentials tested but, as discussed herein, the angular distributions are dependent upon the specifics of the EAM potential parameters. It is important to note that the azimuthal anisotropies (i.e., the ratio of the intensities in the $\phi = -30°$, $+30°$, and 0° directions) are well described by the pair potential. In addition, the intensity in the normal direction ($\theta - 0°$) increases relative to the intensity at $\theta \approx 40°$ as the ejected Rh atom kinetic energy (KE) increases in both the experiment and pair-potential distributions.

Is this improved agreement in the predicted KE distributions fortuitous or is there a sound basis for it? It has been clear to us in the past that the pair-potential description in the surface region is inadequate partly due to the changing number of nearest-neighbor atoms at the

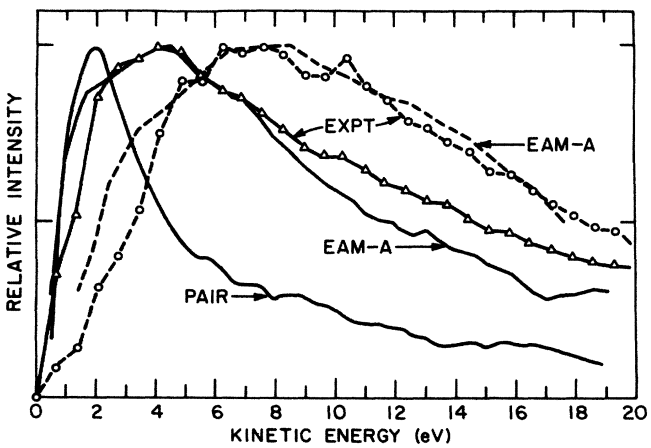

FIG. 2. Experimental and calculated kinetic energy distributions. In all cases the curves are peak normalized. The two experimental curves are the angle-integrated distribution and one at $\phi = -30°$ and $\theta = 40 \pm 3°$. The EAM-A curves are the angle-integrated distribution and one at $\phi = -30°$ and $\theta = 38 \pm 7.5°$. Only the angle-integrated distribution is shown for the pair-potential calculation. The angle-integrated distributions are shown as solid lines and the ones at $\theta \approx 40°$ are dashed lines.

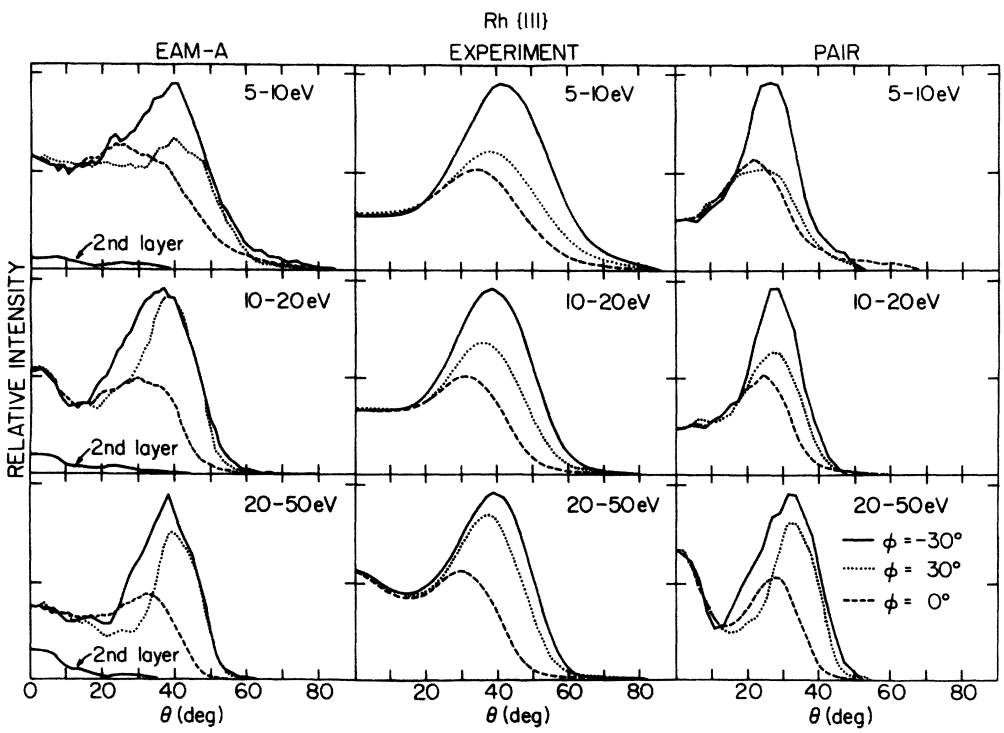

FIG. 3. Polar angle distributions for various azimuthal angles for fixed secondary kinetic energy of the Rh atoms. In each frame the data are normalized to the $\phi = -30°$ peak intensity. For the calculated data the full width at half maximum (FWHM) of the resolution is 15° in the polar angle. A constant solid angle is used in the histogramming procedure. The experimental resolution is approximately the same. The surface normal corresponds to $\theta = 0°$. The curve marked 2nd layer is the polar distribution along $\phi = -30°$ for the ejected second-layer atoms.

interface. Satisfactory solutions to this regime were not forthcoming partially since we did not have the detailed data that exposed the nature of the deficiencies. Contour plots of the energy of one atom ejecting from a site in the Rh{111} surface for the pair and the EAM-A and EAM-C potentials are shown in Fig. 4. There are several features apparent in these plots which have important implications for the particle-ejection process. The surface binding energy of the EAM potentials is larger (5.1–5.3 eV) than that of the pair potential (4.1 eV), even though all of the potentials have been fit using the bulk heat of atomization of Rh of 5.75 eV. It is often suggested that the peak in the KE distribution is proportional to the energy cost to remove an atom from the surface,[17–19] providing a logical explanation for the fact that the peak in the EAM energy distributions occurs at a higher value than for the pair potential. In addition, the EAM potentials are relatively flat in the attractive portion of the entire surface region. There is a 3–4 eV attraction for the ejecting atom even above a neighboring atom. The pair potential has only ~1 eV overall attraction. Thus, particles ejecting at more grazing angles will experience a larger attraction to the surface when moving under the influence of the EAM potential than when moving under the influence of the pair potential. This effect will shift the peak in the KE distribution toward larger values and will bend particles further away from the surface normal, moving the peak in the polar distributions to higher values of θ. Our feeling is that the more planar descrip-

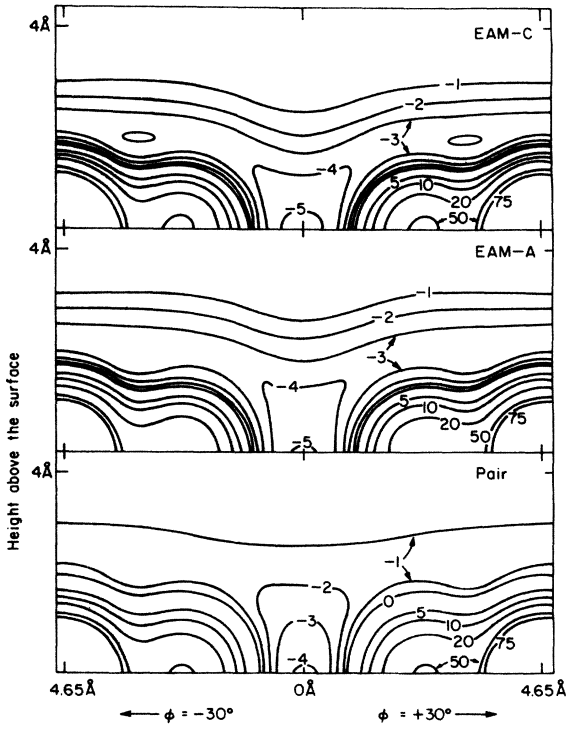

FIG. 4. Contour plots of the potential energy [in eV from Eq. (1)] of a Rh atom ejecting from a Rh{111} surface for the pair potential, EAM-A and EAM-C. The ordinate is the height of the atom above the surface (Å). The abscissa is the position of the atom (Å) along the surface in the $\phi = \pm 30°$ azimuths.

tion of the surface region is more realistic and thus the EAM potential is more appropriate than pair potentials in the surface region.

The larger effective surface binding associated with the EAM description results in fewer particles ejected with low KE's. To a first approximation, then, the change in the features in the energy distribution are a result of a decrease in the magnitude of the peak intensity, resulting in a more prominent high KE tail. This increased binding energy also dramatically affects the total yield. For the pair-potential calculation the calculated yield is 6.1 Rh atoms per incident Ar particle, while for EAM-A the yield is 3.7 atoms per Ar atom. This lower value is closer to the range of experimental yields (see, for example, Ref. 25) than the pair-potential value. Note also that the ratio of the yields between the two methods of calculation is $6.1/3.7=1.6$ whereas the ratio of surface binding energies is only 5.1/4.1 or 1.2. Transport theories of sputtering suggest that the yield is inversely proportional to the binding energy.[25] From our calculations it is clear that the nature of the potential surface also influences the expected yield.

The energy distributions of the atoms that eject into the peak of the polar distribution along $\phi=-30°$ (often called the "spot") are also shown in Fig. 2. The agreement between the experimental and EAM-A distributions is remarkable. This energy distribution peaks at ~ 7 eV whereas the angle-integrated distributions peak at ~ 4 eV. In this energy regime the particles that eject into this "spot" are "hotter" than the particles ejected in other directions.

The angular distributions for three other Rh EAM potentials are given in Fig. 4. Although numerous other potentials were tested, these four (EAM-A, -B, -C, -D) yield the most reasonable distributions and provide a base for determining the parameters which most influence the experimental results. We have subjectively chosen several features of the angular distributions that are important to describe. The first is the shift in azimuthal anisotropy as the Rh atom KE increases. At 5–10 eV (Fig. 3) the $\phi=-30°$ experimental intensity is greater than for the other two azimuths. For 20–50 eV the $\phi=\pm 30°$ intensities are almost equivalent and of greater intensity than the $\phi=0°$ case. The second is that the peak in the $\phi=\pm 30°$ directions should be observed at about 40°. (The peak position along $\phi=0°$ is always less due to increased blocking in this direction.) Finally, in the 20–50 eV range the intensity in the direction normal to the surface ($\theta=0°$) should be approximately half of the peak intensity. From our calculations using pair potentials we believe that a significant fraction of the intensity of the particles ejected in the normal direction at 20–50 eV is due to second-layer atoms that are focused by the three surface atoms surrounding it.[7] Since we ultimately want to examine adsorbates that can either bond directly above a second-layer atom or above a third-layer atom, it is important to be able to describe the ejection of the second-layer atoms reasonably well. Note that the overall ejection is dominated by the first-layer ejection, but in the specific energy and angle space in question the second-layer ejection is important. With these criteria, potential EAM-B is not considered satisfactory since the normal emission intensity at 20–50 eV is too low and the polar angle peak in the 5–10 eV range is $\sim 30°$. Potential EAM-C is deficient since the normal emission is too intense in all energy ranges. Potential EAM-D exhibits weak normal emission in the 20–50 eV range, the polar angle peak position is $<35°$ and the 5–10 eV azimuthal angle distributions are almost isotropic.

Ultimately it is desirable to correlate critical features of the potentials with specific parts of the EARN distributions. This goal is complicated by the fact that the attractive part of the surface potential not only influences the ejection process but also influences the effective size of the atoms. For second-layer ejection the energy barrier that the atom must overcome in moving through the first layer is also important. Finally, the potential influences the dynamics of all of the motions that give rise to energizing an ejecting atom. Given these complexities we have chosen to examine three slices of the potential surface. The first slice is shown in Fig. 4 and indicates the energy required to remove a first-layer atom from the solid from various positions. The second slice is shown in Fig. 5 and indicates the energy of an atom [Eq. (1)] in the second layer as a function of the distance to another second-layer atom. This representation provides an indication of the magnitude of the interaction between atoms within the solid. The final slice is shown in Fig. 6 and indicates the energy of a second-layer atom as it moves upward through the threefold hollow site in the first layer.

We first examine the effect of the magnitude of the barrier on the trajectories of atoms escaping from the second layer. As shown in Fig. 6, potentials EAM-A and EAM-C are constructed with the lowest barriers and, as is evi-

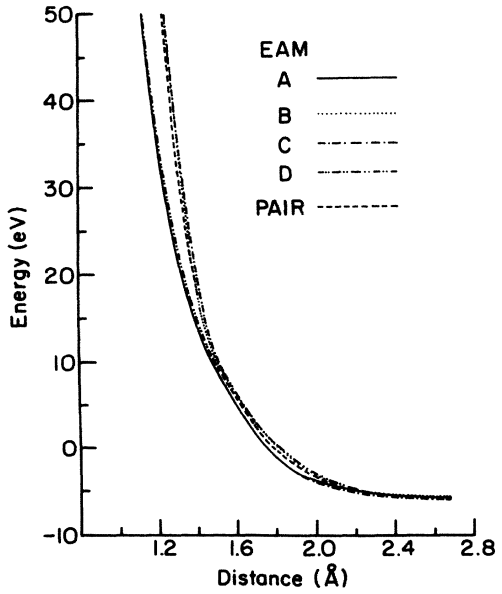

FIG. 5. Energy of an atom in the second layer as a function of the distance to another atom in the second layer for the various potentials. The equilibrium separation is 2.69 Å.

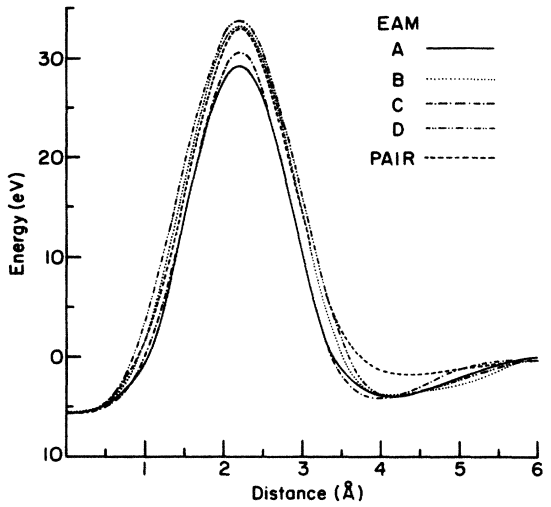

FIG. 6. Energy of an atom in the second layer as it moves vertically through the threefold hollow site in the first layer and towards the vacuum.

dent from Figs. 3 and 7, these barriers result in the largest amount of second-layer ejection for the 20–50 eV particles. As this barrier height is increased as with EAM-B and EAM-D, the second-layer ejection is effectively suppressed. The energy spectrum normal to the surface and the percentage of atoms that eject from below the top layer are particularly sensitive to the barrier height.

The size of the atoms as given by the curves in Fig. 5 also aid in interpreting the EARN distributions. As described in the Appendix, the short-ranged interaction in these EAM potentials is described by the Moliére potentials.[26] There has been considerable debate in the literature as to the appropriate value for the Firsov screening length.[27] We have tested the sensitivity of the potentials to this parameter. For EAM-B, -C, and for the pair-potential calculation, the full Firsov screening length is used. Comparison of results of simulations of keV ion scattering from surfaces has suggested that smaller screening lengths may be more appropriate.[27] Therefore, for EAM-A, -D the Firsov screening length is scaled by 0.9. As a consequence of these changes, for energies above ~ 10 eV (Fig. 5) potentials EAM-B, -C describe effectively larger atoms than EAM-A, -D. For the low-energy region the atoms represented by EAM-B, -D are bigger than EAM-A, -C.

The size of the interactions influences the peak position in the polar angle distribution. The larger the effective size of the atoms, the more the ejecting atom will be deflected towards the surface normal. For example, the angular distributions resulting from trajectories calculated using EAM-B, -D exhibit peak positions closest to the normal. It is EAM-B, -D that are largest in the lower-energy regime, the regime which is apparently most important in determining the polar angle of maximum intensity.

The most serious discrepency between experimental and calculated angular distributions for all of the EAM potentials is that the calculated angular distributions for 5–10 eV and 10–20 eV particles appear to have a $\cos^n\theta$ background ($n \approx 2-3$) that is not apparent in the experimental distributions nor in the calculated pair-potential distribution. Although the reasons for this discrepancy are not yet clear, it is possible that this background is related to the degree of smoothness in the surface of the

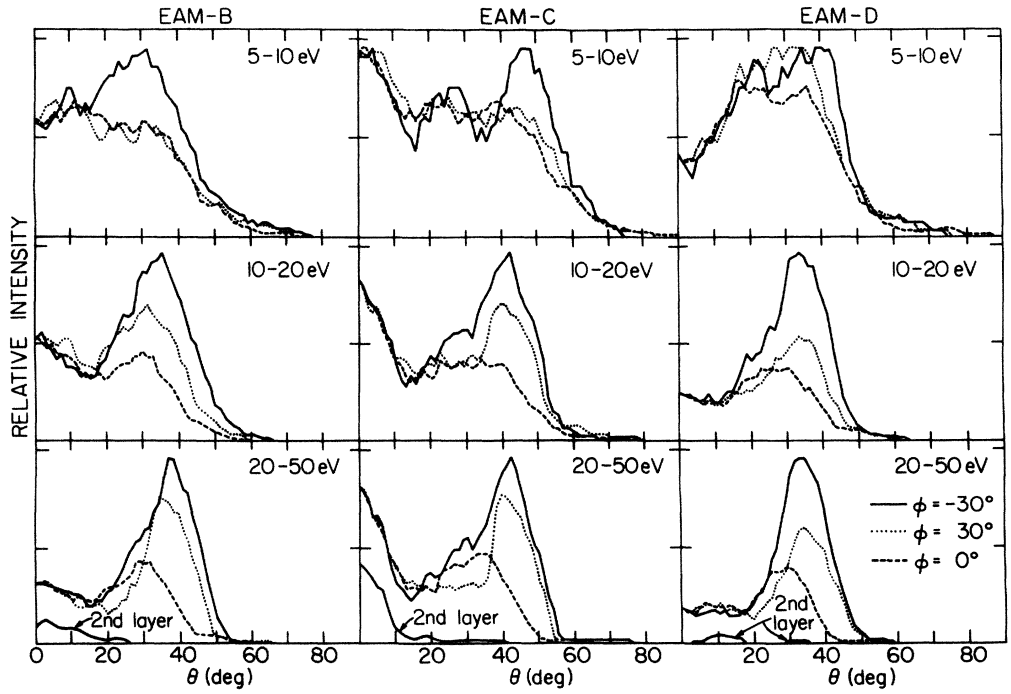

FIG. 7. See the caption to Fig. 3.

EAM potentials. It is possible that future improved descriptions of the surface electron density will further improve the agreement between experiment and theory.

IV. CONCLUSIONS

The energy and angular distributions of Rh atoms ejected from a Rh{111} surface due to keV-Ar-atom bombardment have been modeled with classical dynamics simulations and a many-body EAM potential. We find that the EAM potential significantly improves the agreement between calculated and experimental distributions over previous simulations using a pairwise additive potential. The important differences between the pair and EAM potentials occur in the surface region where the EAM potential predicts a larger surface binding energy and a more planar potential. This effect causes fewer atoms to eject with low kinetic energy and results in an energy distribution which is broader and which peaks at a larger energy than that calculated with the pair potential.

It is apparent that a many-body potential is necessary to quantitatively describe the EARN distributions although the EAM-A potential does not provide a perfect description of the experimental scattering data. Within the embedded-atom method a different prescription for obtaining $F(\rho)$ and $\phi(r)$ may improve the fit. Perhaps a different many-body potential is more appropriate. In any event, a more detailed understanding of how various parts of the potential surface influence the scattering events will undoubtedly improve our understanding of the interaction potential.

ACKNOWLEDGMENTS

The authors greatly appreciate the assistance of M. Daw, S. Foiles, and M. Baskes who provided their computer code for determining forces with the EAM potentials and some embedding functions that were used in the evaluation of the appropriateness of EAM potentials for sputtering. The financial support of the National Science Foundation, the Office of Naval Research, the Air Force Office of Scientific Research, the Foundation Research Program of the Naval Postgraduate School, the Shell Corporation, and the IBM Corporation is gratefully acknowledged. B.J.G. additionally appreciates support from the Camille and Henry Dreyfus Foundation. The Pennsylvania State University supplied a generous grant of computer time for these calculations.

APPENDIX: Determination of $F(\rho)$ and $\phi(r)$

The electron density-dependent part of the total energy $F(\rho)$ was obtained in this work by a fitting procedure that yields a tabulation of $F(\rho)$ over a large number of closely spaced points in ρ space from which an interpolation scheme may be used to evaluate $F(\rho)$ during the dynamics simulation. The specific fitting procedure followed is summarized herein.

(1) A cubic spline of the spherical atomic density function $\rho(r)$ for rhodium was defined using the following input data:

$$\rho(r)=\begin{cases}0, & r\geq 4.23\ \text{Å}\\ \rho_{\text{SCF}}(r), & 0.56\ \text{Å}<r<4.23\ \text{Å}\\ \text{linear with negative slope}, & r<0.56\ \text{Å}\ ,\end{cases}$$

where $\rho_{\text{SCF}}(r)$ is a spherically averaged[13] self-consistent-field density function.[28] The splined region near $r=0$ where $\rho_{\text{SCF}}(r)$ vanishes is necessary to allow the definition of a cubic spline for an inverse density function $r(\rho)$. The local density and the summed nuclear repulsion energy at a lattice site are then

$$\rho(a)=\sum_{m=1}^{n}\rho[r_m(a)],\quad \phi(a)=\sum_{m=1}^{n}\phi[r_m(a)]\ ,$$

where a is the face centered cubic (fcc) lattice constant, n is the number of neighbors, and $r_m(a)$ is the distance to the m^{th} neighbor. In this work, n was large enough to include all neighbors inside a 4.23 Å cutoff range.

(2) An effective pair interaction was constructed representing the energy of an isolated rhodium dimer

$$V(r_{\text{dimer}})=\begin{cases}V_{\text{Morse}}\ (r_{\text{dimer}}), & r_{\text{dimer}}>1.9\ \text{Å}\\ \text{cubic spline}, & 1.48\ \text{Å}\,r_{\text{dimer}}\leq 1.9\ \text{Å}\\ V_{\text{Molière}}\ (r_{\text{dimer}}), & r_{\text{dimer}}<1.48\ \text{Å}\ .\end{cases}$$

The Morse potential was of the form

$$V_{\text{Morse}}(r)=D_e(e^{-2\beta(r-r_0)}-2e^{-\beta(r-r_0)})F(r)\ ,$$

where $F(r)$ is a Tersoff function[29] designed to switch the potential smoothly to zero at the cutoff distance 4.23 Å,

$$F(r)=\begin{cases}\dfrac{1}{2}\left[1-\sin\pi\left[\dfrac{r-4.23\ \text{Å}+\delta}{2\delta}\right]\right], & r\geq 4.23\ \text{Å}-2\delta\\ 1, & r<4.23\ \text{Å}-2\delta\ .\end{cases}$$

The original goal was to use the spectroscopic values of the Rh_2 to determine D_e, β, and r_0 as then the absolute yield of sputtered Rh_2 species could be predicted. Unfortunately, the region of ρ space that is important for the dimer is also important for the surface region, and values of D_e, β, and r_0 appropriate for the dimer resulted in potentials with surface binding energies <5 eV. As discussed in the text, these potentials did not predict the peak position in the experimental energy distribution, and thus at this time we use D_e, β, and r_0 as parameters. The value of δ used was 0.772 Å. The Molière potential $V_{\text{Molière}}$ is described in Ref. 26.

(3) A region of ρ space (ρ_1, ρ_2) containing the equilibrium density ρ_0 of solid fcc rhodium was defined by a $\pm 10\%$ contraction (expansion) of the lattice constant around its equilibrium value of 3.80 Å. Given $\phi(r)$, $F(\rho)$ may be defined in this region by using the universal equation of state described by Rose *et al.*[30] to determine the

total energy of the solid and requiring equality between this and the EAM total energy expression:

$$E(a)=-E_s(1+a^*)e^{-a^*}=F[\rho(a)]+\tfrac{1}{2}\phi(a)\ ,$$

where

$$a^*=\left[\frac{a}{a_0}-1\right](9B\Omega/E_s)^{1/2}\ .$$

Here, E_s is the equilibrium sublimation energy, a_0 is the equilibrium lattice constant, B is the bulk modulus, and Ω_0 is the equilibrium volume per atom.

(4) A trial nuclear repulsion $\phi(r)$ was chosen to have the form[14]

$$\phi(r)=\frac{Z(r)^2}{r}\ ,$$

where

$$Z(r)=Z_0(1+\epsilon e^{rv})e^{-ar}\ .$$

The crystal elastic constants c_{11}, c_{12}, c_{44}, and the vacancy-formation energy E_{1v}^f may be calculated given $F(\rho)$ and $\phi(r)$.[14] Using the definition of $F(\rho)$ in step (3) and the trial $\phi(r)$, the adjustable parameters a, ϵ, and v in $\phi(r)$ were fit using a nonlinear least squares technique to the reasonable elastic constants and the vacancy formation energy of fcc rhodium. Since c_{11} and c_{12} are related through the bulk modulus which appears in the equation of state, the fit was made to c_{11}, c_{44}, and E_{1v}^f. The parameter values used in this work were $\alpha=2.105$, $\epsilon=2.510$, and $v=1.387$.

(5) The final $F(\rho)$ was defined as a cubic spline of a composite of three functions

$$F(\rho)=\begin{cases}\frac{1}{2}[V(r_{\text{dimer}})-\phi(r_{\text{dimer}})]\ , & \rho\le\rho_1\\ E(a)-\frac{1}{2}\phi(a), & \rho_1\le\rho\le\rho_2\\ \text{linear}, & \rho>\rho_2\ .\end{cases}$$

In the $\rho\le\rho_1$ region, the inverse atomic density function $r(\rho)$ must be used to relate ρ space and r_{dimer}-space. In the $\rho_1\le\rho\le\rho_2$ region, the relation of ρ to the lattice constant a as defined in step (1) is needed.

(6) The final $\phi(r)$ is expressed as a cubic spline defined from points in

$$\phi(r)=V(r)-2F[\rho(r)]\ .$$

This step is necessary to make the EAM total energy expression consistent with the effective pair of interaction, $V(r)$. This definition of $F(\rho)$, $\rho(r)$, and $\phi(r)$ ensures that dimerlike species interact with an effective pair potential $V(r_{\text{dimer}})$, and also that the bulk behavior is properly described. In addition, we have control over the size of the short-ranged close encounter region.

[1] J. B. Gibson, A. N. Goland, M. Milgram, and G. H. Vineyard, Phys. Rev. **120**, 1229 (1960).
[2] M. T. Robinsen and I. M. Torrens, Phys. Rev. B **9**, 5008 (1974).
[3] D. E. Harrison, Jr., J. P. Johnson III, and N. S. Levy, Appl. Phys. Lett. **8**, 33 (1966).
[4] B. J. Garrison and N. Winograd, Science **216**, 805 (1982).
[5] M. H. Shapiro, P. K. Haff, T. A. Tombrello, D. E. Harrison, Jr., and R. P. Webb, Radiat. Eff. **89**, 243 (1985).
[6] D. Y. Lo, M. H. Shapiro, and T. A. Tombrello, Mater. Res. Soc. Symp. Proc., **174**, 449 (1987).
[7] B. J. Garrison, N. Winograd, C. T. Reimann, and D. E. Harrison, Jr., Phys. Rev. B **36**, 3516 (1987).
[8] R. A. Gibbs, S. P. Holland, K. E. Foley, B. J. Garrison, and N. Winograd, Phys. Rev. B **24**, 6178 (1981).
[9] J. P. Baxter, G. A. Schick, J. Singh, P. H. Kobrin, and N. Winograd, J. Vac. Sci. Technol. **4**, 1218 (1986).
[10] G. A. Schick, J. P. Baxter, J. Singh, P. H. Kobrin, and N. Winograd, in *Secondary Ion Mass Spectrometry-SIMS V*, Vol. 44 of *Springer Series in Chemical Physics* edited by A. Benninghoven, R. J. Colton, D. S. Simons, and H. W. Werner (Springer-Verlag, New York, 1986), p. 90.
[11] N. Winograd, P. H. Kobrin, G. A. Schick, J. Singh, J. P. Baxter, and B. J. Garrison, Surf. Sci. **176**, 1817 (1986).
[12] M. S. Daw and M. I. Baskes, Phys. Rev. Lett. **50**, 1285 (1983).
[13] M. S. Daw and M. I. Baskes, Phys. Rev. B **29**, 6443 (1984).
[14] S. M. Foiles, M. I. Baskes, and M. S. Daw, Phys. Rev. B **33**, 7983 (1986).
[15] B. W. Dodson, Phys. Rev. B **35**, 880 (1987).
[16] S. P. Chen, A. F. Voter, and D. J. Srolovitz, Phys. Rev. Lett. **57**, 1308 (1986).
[17] B. J. Garrison, N. Winograd, D. Lo, T. A. Tombrello, M. H. Shapiro, and D. E. Harrison, Jr., Surf. Sci. **180**, L129 (1987).
[18] M. W. Thompson, Philos. Mag. **18**, 377 (1968).
[19] R. Oliva, R. Kelly, and G. Falcone, Nucl. Instrum. Methods **B19–20**, 101 (1987).
[20] M. W. Finnis and J. E. Sinclair, Philos. Mag. A **50**, 45 (1984).
[21] M. Manninen, Phys. Rev. B **34**, 8486 (1986).
[22] J. K. Norskov, Phys. Rev. B **26**, 2875 (1982).
[23] K. W. Jacobsen, J. K. Norskov, and M. J. Puska, Phys. Rev. B **35**, 7423 (1987).
[24] R. Car and M. Parrinello, Phys. Rev. Lett. **55**, 2471 (1985).
[25] P. Sigmund, Phys. Rev. **184**, 383 (1969).
[26] I. M. Torrens, *Interatomic Potentials* (Academic, New York, 1972).
[27] B. Poelsma, L. K. Verheij, and A. L. Boers, Surf. Sci., **64**, 554 (1977).
[28] E. Clementi and C. Roetti, *Atomic Data and Nuclear Data Tables* (Academic, New York, 1974) Vol. 14, Nos. 3 and 4, p. 231.
[29] J. Tersoff, Phys. Rev. Lett., **56**, 632 (1986).
[30] J. H. Rose, J. R. Smith, F. Guinea, and J. Ferrante, Phys. Rev. B **29**, 2963 (1984).